AirTouch: 3D-printed Touch-Sensitive Objects Using Pneumatic Sensing

Carlos E. Tejada[1] ct@di.ku.dk
Raf Ramakers[2] raf.ramakers@uhasselt.be
Sebastian Boring[3] sebo@create.aau.dk
Daniel Ashbrook[1] dan@di.ku.dk

[1]University of Copenhagen
Department of Computer Science
Copenhagen, Denmark

[2]Hasselt University
Expertise Centre for Digital Media
Hasselt, Belgium

[3]Aalborg University
Department of Architecture, Design, and Media Technology
Copenhagen, Denmark

(a) (b) (c)

Figure 1: AirTouch augments 3D-printed objects to enable touch-sensitivity. It works by detecting the pressure change resulting from users blocking tiny air outlets fabricated into the objects. (a) Three active animal objects: each has touch points on its ear, nose, foot, and back. The same machine learning model works interchangeably with all three. (b) Structure inside the bunny, illustrated via computer rendering. The external solid object is shown as clear, while the internal hollow tubes are rendered in translucent blue. (c) The AirTouch-enabled bunny with interactive locations on the ear, nose, back and feet. When the user touches any of these locations, the respective label is displayed.

ABSTRACT

3D printing technology can be used to rapidly prototype the look and feel of 3D objects. However, the objects produced are passive. There has been increasing interest in making these objects *interactive*, yet they often require assembling components or complex calibration. In this paper, we contribute *AirTouch*, a technique that enables designers to fabricate touch-sensitive objects with minimal assembly and calibration using pneumatic sensing. AirTouch-enabled objects are 3D printed as a single structure using a consumer-level 3D printer. AirTouch uses pre-trained machine learning models to identify interactions with fabricated objects, meaning that there is no calibration required once the object has completed printing. We evaluate our technique using fabricated objects with various geometries and touch sensitive locations, obtaining accuracies of at least 90% with 12 interactive locations.

CHI '20, April 25–30, 2020, Honolulu, HI, USA.

ACM ISBN 978-1-4503-6708-0/20/04 ...$15.00.
http://dx.doi.org/10.1145/3313831.3376136

CCS Concepts

•**Human-centered computing** → **Interaction devices;** •**Hardware** → **Tactile and hand-based interfaces;**

Author Keywords

3D printing; pneumatic sensing; touch interaction

INTRODUCTION

Over the past decade, additive manufacturing has moved from industry to desktop-sized 3D printers that empower makers to produce intricate three-dimensional shapes. In contrast to this new ease of producing forms, making interactive and responsive objects usually requires inserting electronic circuitry [22, 27] and thus requires engineering expertise and assembly effort. Similarly to Willis et al. [37], we envision

what we call *print-and-play*: a future where interactive objects are ready to use immediately after fabrication, without extra effort on the maker's part. Such a capability will empower makers, designers, researchers, and educators to instantly turn passive fabricated forms into interactive artefacts. While recent research has made some progress towards this goal [20, 31, 33, 35], these projects still fall short of being purely print-and-play: they require per-user [31] or per-object [20,35] training, are susceptible to environmental interference [12, 33, 35], or significantly alter the object's external form [33].

In this paper, we present *AirTouch*, a novel technique for fabricating touch-sensitive objects that are instantly responsive after 3D printing without the need for assembly or calibration. Our technique minimally modifies the form of the object, adding only a tiny hole to each touch location and inlets for an external source of air and a barometric pressure sensor; when a user touches a hole, the air pressure inside the object changes in a predictable way. AirTouch-enabled objects can be fabricated as a single structure on consumer-level resin-based 3D-printers, without the need for any post-hoc assembly, and can enable up to 12 different interactive locations on fabricated objects.

To summarize, this work contributes:

- *AirTouch*, a novel technique for fabricating objects that are instantly touch-sensitive after printing by measuring differences in air pressure inside the object;
- a characterization of the number of interactive locations that can be enabled with our technique, and its performance; and
- a set of applications that demonstrate AirTouch's potential.

RELATED WORK

AirTouch builds on prior research on prototyping and fabricating interactive objects, and research around pneumatic interfaces.

Prototyping and Fabrication of Interactive Objects

A growing body of literature has explored different techniques to fabricate interactive objects. While Ballagas et al. offer a comprehensive overview of this design space, grouping previous endeavours according to the interaction mechanism used [1], this section emphasizes the progress of these previous efforts towards being print-and-play. Two properties of the object production process strongly influence the amount of post-printing effort needed: the degree of assembly or other physical modification required to enable interactivity, and whether a machine-learning training phase is necessary—and if so, how much. Independent of the print-and-play nature of an object, the amount of effort required from the user to interact is also worth considering.

Some early research on prototyping interactive objects focused on adding interactive functionality to the objects rather than on simple methods for fabrication. For example, some systems require assembling electronics and other components inside a printed shell [9, 16, 26, 27] and others require casting silicone [8, 24].

Other approaches require less assembly. Some research has detected changes in acoustical signals caused by user manipulation of geometry [14, 15, 28]; however, the requirement for complex or movable geometry can mean considerable post-print effort for cleaning, assembling, and gluing.

Some recent work has come much closer to the print-and-play ideal, enabling interactivity with significantly less or no post-print manipulation. One approach is to use multi-material printers to enable capacitive touch sensing [6, 30, 31] or optical sensing [37]; however, these approaches require attachment of multiple points of circuitry or optic sensors to operate, and the size of object is limited. Another optical approach is to use computer vision to detect user interaction [32]; however, cameras are prone to problems with occlusion (i.e., touches on the back of an object cannot be detected, nor can touches hidden by the hand itself), and it is difficult to differentiate touching from merely being close to the object.

Several projects require nearly no post-print manipulation. Touch & Activate [20] used an affixed microphone and speaker to detect how acoustic sweeps were changed by user touch; this technique worked with many objects, including off-the-shelf ones, but required a new machine-learning model to be trained for every object. Blowhole [35] used the sound produced by users blowing into differently shaped cavities to determine interaction location; the objects were ready to interact with immediately after printing. While Blowhole used a mathematical model for training-free operation, it could only recognize six locations, and the 5 mm-diameter holes disrupted object surfaces. Tickers and Talker [33] used centimeter-scale physical markers which made unique sounds when plucked, but significantly impact the geometry of the object. INTACT [10] uses a 3D model of an object placed on a 6-axis force sensor to mathematically determine where the user is touching. While it can sense touch with high precision, objects are limited in size to around 20 cm, and require recalibration after moving.

In contrast to this previous work, AirTouch has several advantages. It needs nearly no post-fabrication assembly or other manipulation: the user simply plugs in one or two tubes, depending on the particular configuration. It requires no per-object training: as we demonstrate in a later section, pre-trained machine learning models transfer between different objects with high accuracy. AirTouch has little constraint on size, working at scales as small as 4 cm and as large as 2 m. Unlike some previous work, AirTouch does not significantly disrupt the surface of the object with new geometry, and AirTouch-enabled objects can be held in the hand without interfering with recognition.

Pneumatic Input for Interaction

AirTouch's use of air pressure as its sensing mechanism is inspired by other pneumatic interaction work. A number of projects have used pneumatic techniques to augment the digital fabrication process, aiming to reduce fabrication time by

inflating objects to their final form [21,25,38], or to add movement to otherwise static objects [18, 19, 39].

Various researchers have investigated the use of pressure as an input mechanism. Most use sensing of pressure inside flexible enclosures, including buttons [5, 7, 36], computer mice [13], robots [34], and balloons [17]. Due to measuring the pressure of air trapped inside a flexible structure, these systems are limited to sensing one interaction location, and can suffer from ambiguity if the user presses with different levels of force. In contrast, AirTouch's use of rigid object enables sensing up to 12 different interaction points, and it can operate reliably, independent of the user's pressing force on those points.

AIRTOUCH OVERVIEW

AirTouch makes use of some of the basic principles of fluid behavior. In particular, we use the *principle of continuity* [23]—which indicates that the total flow of air exiting an object must equal the flow of air entering the object—and Bernoulli's principle [2], which relates flow and pressure. In combination, these two principles predict that when there is a change in the size of an opening through which fluid is passing, the pressure will vary in response. Our objects are therefore comprised of a series of pressurized tubes with uniquely sized outlets. Covering an outlet changes the amount of area through which air can escape, and thereby changes the pressure in the object. In the following, we sketch some of the mathematical theory of operation that enables AirTouch to function.

Theory of Operation

The behavior of AirTouch can be approximated with principles from fluid dynamics. By the continuity principle—that the total output from a system must be equal to its input—we know that Q_I, the flow of air entering the object, is equal to $\sum Q_i$, the total flow coming out of all openings. The relationship of flow to the cross-sectional area A of an opening is given by Bernoulli's principle [23], allowing flow to be expressed as

$$Q = CA\sqrt{\Delta P} \tag{1}$$

where C is a constant incorporating an adjustment for the shape of the orifice, the density of air, and other unknowns, and ΔP is the difference in pressure before and after the opening. We can now use Equation 1 to express and simplify the continuity equation in terms of the sum of the areas of each outlet i and the difference in pressure between the inside of the object and the atmosphere:

$$\begin{aligned} Q_I &= \sum Q_i \\ &= C\sum A_i \sqrt{\Delta P} \end{aligned} \tag{2}$$

Now consider the situation where we cover one outlet. Because of continuity, the input flow (held constant by the air compressor and regulator valve) and output flow are identical to when no outlets are blocked. Therefore, the pressure inside the object must increase to compensate for the decreased total discharge area. Assuming we have blocked outlet x, we now have

$$C\sum A_i \sqrt{\Delta P} = C\left(\sum A_i - A_x\right)\sqrt{\Delta P_x} \tag{3}$$

illustrating that with a smaller total area we must have a new, larger pressure ΔP_x. Solving Equation 3 for ΔP_x allows us to predict the new pressure that will result from covering an outlet of cross-sectional area A_x:

$$\Delta P_x = \frac{(\sum A_i)^2 \Delta P}{(\sum A_i - A_x)^2} \tag{4}$$

or, equivalently, given a pressure change of ΔP_x, the outlet area which resulted in that pressure change:

$$A_x = \sum A_i \left(1 - \sqrt{\tfrac{\Delta P}{\Delta P_x}}\right) \tag{5}$$

As presented here, these fluid dynamics equations work with incompressible, steady flows—that is, liquids flowing in steady state—and perfectly shaped outlets of known geometry. Our system does not hold to these constraints: 3D-printed objects, and thereby our outlets, are not perfect; air is compressible; and our objects are subject to internal turbulence due to their complex geometry (see Figure 1b). Due to these factors, the above equations do not perfectly match our observed data, but provide guidelines for understanding and predicting the general behavior of the system.

Internal Structure

AirTouch adds an internal structure to 3D models that distribute incoming flow from an air compressor to outlets on the object's surface (Figure 1b). This internal structure consists of several components: a central flow-distribution chamber which supplies all tubes with air; an inlet via which the air source provides pressurized air flow to the flow-distribution chamber; a connection point for the pressure sensor; a series of tubes that connect the flow-distribution chamber to touch locations on the object's surface. By using this structure in all AirTouch-augmented objects, we ensure that the pressure increases when touching the same outlet are comparable, regardless to the outer geometry of the augmented object.

Sensing User Interactions

The basic user interaction with an AirTouch-enabled object is via touch. When a user touches one of the outlets on the object's surface, the airflow through that outlet is blocked. As each outlet has a different size, the airflow through each outlet is unique and is proportional to the outlet area (Equation 2). Blocking the flow from an outlet causes a identifiable rise in the barometric pressure inside the object. Our system records these changes in air pressure using a barometric sensor, and translates them to an outlet ID, and subsequent position on the object's surface. Figure 2 shows an abstract representation of the unique barometric increases sensed when the user covers different outlets, and Figure 3 shows actual sensed touch data.

PARAMETER EXPLORATION

Every AirTouch object contains a flow-distribution chamber, tubes, and outlets. In this section, we report on the design and fabrication of this internal structure based on literature and additional testing. Our design decisions were guided by

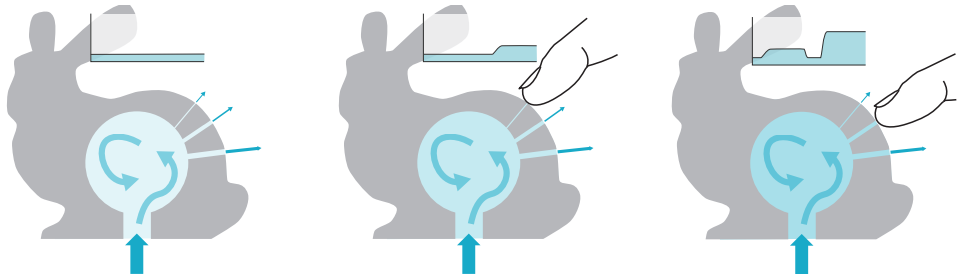

Figure 2: Representation of AirTouch's working principle. When an outlet is covered, the barometric pressure inside the fabricated object rises to an identifiable level. As each outlet is unique in size, covering different outlets yields a different barometric pressure response.

the following three requirements: (1) the object, including the internal structure, must be fabricatable with a consumer-level 3D printers; (2) the outside geometry of the object cannot be modified; (3) per-object calibration is not allowed.

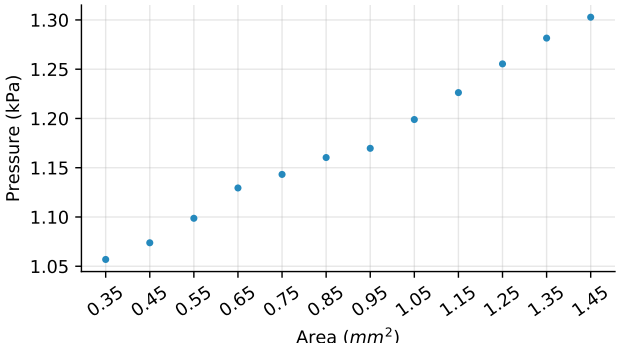

Figure 3: Pressure in kilopascals (kPa) for single touches on twelve differently sized outlets (ranging in cross-sectional area from .35 mm^2 to 1.45 mm^2 in .1 mm^2 increments).

Experimental Setup

We constructed a test setup consisting of a JunAir 2000-40PD air compressor, Festo MS4-LR-1/4-D5-AS valve, and an analog Panasonic PS-A (ADP5) barometric sensor. The sensor is connected to an Arduino Uno, which samples the air pressure at 5 kHz. We connect standard air compressor tubing (polyethylene, 6 mm diameter) to the valve, and the barometric sensor to the object. This sensor is responsible for detecting the subtle pressure changes in the system caused by user interactions, and can sense pressures relative to atmospheric pressure from 0 to 6 kiloPascals (kPa). The sensor's limited operating range requires that we empirically set the valve's value for objects having a different number of outlets to avoid saturation. To reduce the noise from the sensor readings, we filter the incoming signal using the 1€ Filter [4] using β and cutoff values set empirically, dependent on the base pressure output of the compressor.

We print our objects using the FormLabs Form 2 3D printer, a consumer-level resin-based stereolithography (STL) printer capable of high resolutions. We use STL technology because in our initial experiments, it became clear that current FDM-based printers are not capable of precisely printing tiny holes at arbitrary orientations. We print AirTouch-enabled objects as single structures with no assembly needed. The only addition to the standard post-processing required of all STL print processes is a 30-second flushing stage with the air compressor immediately after printing to prevent residual resin causing blockages during curing.

Flow-Distribution Chamber

AirTouch objects embed a spherical flow distribution chamber to distribute incoming flow between between tubes; 3D printing small-size spherical shapes does not require support material. Instead of using a flow distribution chamber, we also experimented with hollowing the object. In these shell structures, outlets are simply holes and do not require tubes. This approach, however, requires per-object touch calibration while also requiring higher pressures for operation, as the air flows through the entire geometry of the object. In contrast, the spherical flow-distribution chamber has the same shape across objects and ensures a consistent airflow. To allow touch interactivity on small objects with AirTouch, the flow-distribution chamber should be small to fit objects of various geometries. Therefore, we fabricated three Stanford bunnies, each with identical outlet configurations but with varying flow-distribution chamber diameters of 15, 20 and 30 mm in diameter. We recorded the barometric pressure changes when covering the outlets and found that the volume of the chamber does not significantly impact the relative pressure variations between outlets. We did find, however, that smaller cavities yield a higher noise profile on the resulting signals; therefore, as a compromise between size and performance, we used flow-distribution chambers of 30 mm diameter in most of our further experiments.

Tubes

The touch locations on the object's surface are connected to the flow-distribution chamber with cylindrical tubes. To allow tubes to be embedded in small objects, we want the diameter to be as small as possible. After experimenting with different diameters, we picked 5 mm tubes as the best tradeoff between size and printability. While 3 mm tubes often worked, we

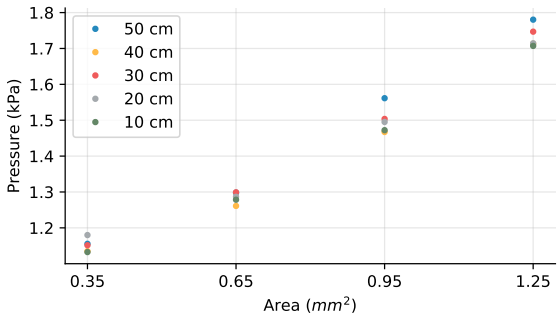

Figure 5: Pressure results by tube length. Note that the pressure difference between tube lengths is significantly smaller than the difference between touches on outlets of different sizes.

found that with this smaller size it was difficult to guarantee that all of the resin would drain from the tubes before post-print curing.

Based on fluid dynamics literature [3], we determined that the length of the tube as well as the area of the outlet influences the barometric pressure inside the object. First, we tested if varying the tube length produces enough difference in barometric pressure to identify the tube from which the airflow is blocked. To do so, we fabricated three objects of varying geometries: a duck, a bunny and a CHI-nosaur. Each has a 30 mm-diameter chamber and four outlets, placed at the foot (.35 mm^2), nose/beak (.65 mm^2), ear (.95 mm^2), and back (1.25 mm^2). Although these objects share the same cavity size and outlet configuration, their interior tube lengths vary between 3–100 mm. Figure 4 shows no significant difference in pressure responses when covering each of the outlets for all three objects. In the next section, we report on testing the impact of varying the area of the outlet.

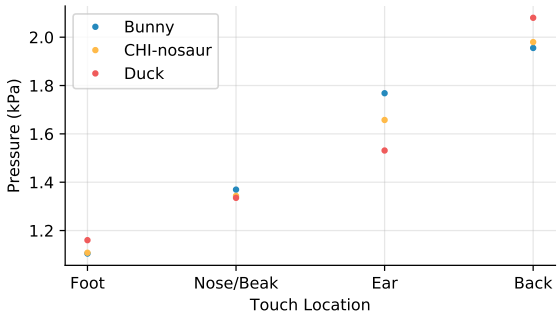

Figure 4: Pressure results by location on interactive animals. Note that the pressure difference between animal models is significantly smaller than the difference between touches on outlets of different sizes.

Although we did not find significant difference between the pressure increases from interacting with desktop-sized objects of different geometries, we wished to identify the potential size limits of our technique. Because our available printers are limited in size, we used 6 mm polyethelyne (PE) tubing (hardness: Shore D 52) to simulate printed channels. We fabricated a standalone flow-distribution chamber of 30 mm diameter with four 6 mm outlets. We also fabricated four 6 mm tube caps with outlets of the same sizes as the animals listed above. We connected one 50 cm length of tube to each outlet, terminating each with one cap, and recorded the pressure for each. We repeated this procedure four more times, shortening the tube length by 10 cm each time. Figure 4 illustrates our results: we see very little impact of tube length on pressure. As an additional informal experiment, we connected one outlet to a 40 m-long tube. At this length, the volume of air in the tube is significant (2 L) and is subject to both compression and losses due to friction [3]. Due to these effects we see a noticeable 2–3-second delay for the pressure to reach its full amplitude. While not suitable for interactions requiring immediate responsiveness, this example shows the versatility and scalability of our technique. Although these experiments suggests that AirTouch is capable of augmenting larger objects, more experimentation is still needed.

Outlets

In contrast to varying the length of the tubes, we did observe a significant difference in the barometric pressure response when blocking the airflow from tubes having different outlet diameters. To minimally disturb the object's original geometry and ensure outlets are always covered entirely when touched, we wanted to use outlets with diameters as small as possible. During our initial exploration phase, we found that our printer was unreliable in printing outlets smaller than 0.6 mm in diameter. Additionally, we observed that the difference between barometric pressure responses of small outlets are not significant in the presence of large outlets. Therefore, we empirically set the maximum outlet diameter to 1.50 mm.

With an operational range of 0.6–1.50 mm for outlet diameters, we optimized the step size between outlet diameters to maximize the number of outlets while ensuring significant differences between barometric pressure responses from all outlets. Equation 5 indicates that the pressure/area relationship is nearly linear for our range of diameters. We printed three test objects, each with outlets in the operational diameter range but with area steps of 0.02, 0.06, and 0.1 mm^2 between subsequent outlets. We then connected each to the testing setup and recorded touches on each outlet. We found that with the smaller area increments, the pressure change between neighboring outlet sizes was insufficient to offer a clear separation in the presence of sensor noise (approximately 0.01 kPa). Therefore, all of our subsequent objets are printed with at least a 0.1 mm^2 separation between hole areas. Table 1 illustrates, at actual size, the final set of 12 outlet dimensions we use.

As discussed earlier, the tubes connecting the outlets to the chamber are 5 mm in diameter to prevent clogging. We therefore reduce the last 1 mm of the tube to form the outlet, as shown in Figure 6.

0.334	0.378	0.418	0.455	0.489	0.52	0.55	0.578	0.605	0.631	0.656	0.679

Table 1: Final outlet dimensions shown at actual size with radius in millimeters indicated under each. The area increases by .1 mm^2 between each subsequent hole, ranging between 0.35–1.45 mm^2.

Figure 6: Close up view of the connection between the tube and the outlet.

SOFTWARE

In this section, we discuss the algorithms for recognizing and identifying touches as well as the software implementation that facilitates designing AirTouch's internal tube structure.

Designing AirTouch Objects

AirTouch-enabled objects require an object's internal structure to be augmented with an inlet for pressurized air, a flow-distribution chamber, uniquely sized outlets at desired touch locations, and a connection for the sensor. To facilitate designing AirTouch objects, we created an Autodesk Meshmixer script which automatically modifies the model's internal structure and adds appropriately-sized outlets to objects at user-selected locations. Our script embeds a flow-distribution chamber inside the model, and uses the tube routing algorithm described in [29] to attach a tube spanning from the cavity to locations selected by the designer. If more precision is necessary, tubes can be added manually to objects using standard CAD software.

Touch Recognition and Identification

In order to identify when an outlet is covered, we first segment the signal coming from the sensor into 100-sample windows. We then calculate the mean and standard deviation for each window, and once the standard deviation surpasses an empirically set threshold, we assume there has been a touch or release event. To identify whether this change has been a touch or a release, we compare the mean of the current window with the mean of the previous one: if the current mean is higher than the previous, an outlet has been covered; if not, an outlet has been released.

Once we have determined that a touch event has happened, we identify which outlet has been covered. We take the mean of the 1000 samples previous to the touch event as the pressure baseline, and divide it by the mean of the 1000 samples following the touch. This ratio compensates for drift in the signal caused by minor atmospheric fluctuations and imprecisions in the regulator valve.

PERFORMANCE TESTING

To show the viability of AirTouch, we evaluated our recognition pipeline on a set of AirTouch-enabled objects of varying geometries and outlet configurations: an interactive bar chart, a Stanford bunny, a color hue selector and a dual-touch sensing sphere. For each outlet configuration, we train a machine learning model (SVM with rbf kernel) using a single instance consisting of mean and standard deviation for the registered pressures for a given touch. We proceed to cycle through the outlets of each object, recording the classification result for each touch. We repeat this process four times per object.

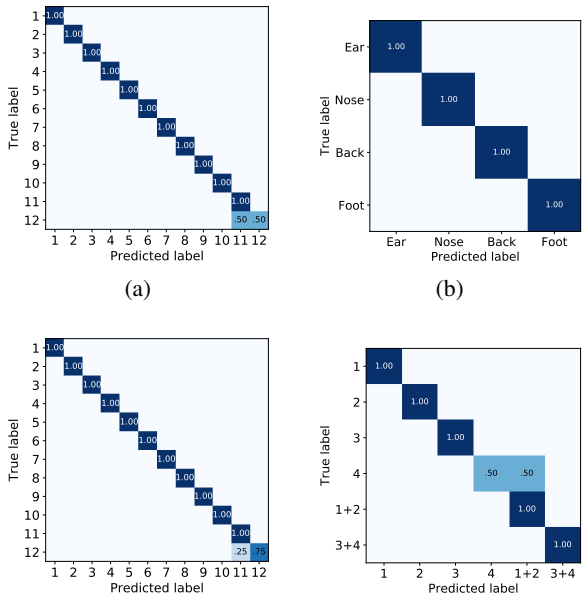

Figure 7: Confusion matrices of classification accuracies from our tests: interactive bar plot (a); augmented Stanford bunny (b); color hue selector (c); grasp-sensing sphere (d). Each cell indicates the number of classified touch interactions to a predicted class (row) for each actual class (column).

We obtained average accuracies of 95.5% (for the bar chart), 100% (Stanford bunny), 97.75% (color hue selector), and 91.6% (Grasp sensing cube). Figure 7 shows a detailed view of the performance for each object.

EXAMPLE DESIGNS AND APPLICATIONS

Because its ease of fabrication, and large number of interactive locations, AirTouch lends itself to the rapid prototyping of interactive devices. Below we present a number of example usages of AirTouch which illustrate its potential. All applications are developed in C# and WPF and receive data (over a socket connection) from Python code running the touch detection described above.

(a) (b) (c) (d)

Figure 8: Example AirTouch Applications. With AirTouch, interactive objects are fabricated as a single structure without any post-print assembly or calibration. We showcase objects of different geometries augmented with AirTouch: an interactive bar chart (a); interactive animals (b); grasp-sensing sphere (c); and a color hue selector (d).

Interactive 3D Bar Chart

Recent work has highlighted the benefits of data physicalization [11]. We designed a three-dimensional bar plot displaying the relation between the submitted and accepted papers in the past four years to CHI, UIST, and TEI (Figures 1c and 8a). To obtain more information about the proceedings, the user touches the top of a bar, and the companion application shows the acceptance rate, number of accepted papers for the year and conference in question.

Interactive Animals

AirTouch can identify interactions on objects of varying geometries, but with the same outlet configurations, with a single, pre-trained machine learning model. We fabricated a set of interactive animals of different outer geometries, but sharing the same outlet configuration (i.e., an ear of different animals has the same outlet diameter). We augmented a Stanford bunny, a duck, and a CHI-nosaur with interactive locations on the nose, ear, back and leg. When a location is touched, the corresponding label is displayed (Figure 8b).

Grasp Sensing

To showcase AirTouch's dual-touch sensing capabilities, we developed a touch-sensing sphere (Figure 8c). We augmented a sphere with four touch locations throughout its surface. When an outlet is covered, the companion application highlights which face is touched. When two outlets are covered simultaneously, the system highlights both faces.

Color Hue Selector

AirTouch can enable up to 12 interactive locations on 3D-printed objects. We designed a circular color hue selector for a drawing application (Figure 8d). The user selects a color using the selector, and sketch in the drawing window.

DISCUSSIONS AND LIMITATIONS

While AirTouch is successful in fabricating touch-sensitive objects and tangible input components without the need of any post-print assembly it has limitations. The most obvious one is the need for an air compressor to power the fabricated objects. Although we employed an air compressor to power our fabricated objects, other air sources might be used, granted they guarantee a constant stream of air. A miniature air pump, similar to the one used by Vázquez and collaborators in [36], can power AirTouch-enabled objects given their low pressure requirements.

Another limitation of our technique is that it's only able to augment objects fabricated using high-resolution 3D-printing technologies. We explored fabricating AirTouch-enabled objects using Fused Deposition Modeling (FDM) printers, but encountered a number of issues. Because of its layer-by-layer fabrication procedure, some objects fabricated with our Lulzbot Taz 6 and QiDi Technology X-One presented significant leaks in the internal structure of the object, hindering the technique's performance. We plan to explore the effects of employing smoothing techniques (e.g., acetone smoothing), and varying the shell thickness of the model when printing to reduce leaks. FDM printers also lack the precision of STL printers, meaning that when printing outlets. Future work can explore the different approaches to ensure the correct fabrication of outlet sizes on lower resolution equipment.

Although we experienced a noticeable latency in our 40m-long tube experiments between when covering the outlet and the signal reaching its full amplitude, these effects were not present in AirTouch-enabled objects—the pressure increase upon covering an outlet was instant. Future work can explore the use of our technique to enable richer gestures such as swiping and sliding on fabricated objects.

Employing the same principle used to detect individual touches, AirTouch can identify up to two simultaneous touches on different locations throughout the fabricated object. Because the increase in pressure is proportional to the outlet area, covering multiple outlets can be identified as a new touch location—as long as the sum of the areas of the covered outlets results in a unique change in pressure. In order to guarantee a 0.1 mm^2 separation between the outlets and their respective combinations, we used outlets sizes of 0.4 mm^2, 0.5 mm^2, 0.6 mm^2, and 0.8 mm^2 in our test objects.

Finally, we experienced small variations in the measured barometric pressures inside our fabricated objects when compared to previous days. This is due to the everyday changes in environmental barometric pressure. To evaluate the effects of these everyday changes in our system's performance we per-

formed a preliminary test over a period of four consecutive days where the ambient pressure varied from 0.1 to 0.7 kPa. Using the bunny model, we recorded touches each day and found that the pressure variation shifted the baseline of the measurements by an amount smaller than the separation between different touches.

CONCLUSION

In this paper we introduced AirTouch: a technique for fabricating touch-sensitive objects without the need of any post-print activities such as assembly or calibration. We presented the theory behind AirTouch, our explorations of parameters for both interaction and successful fabrication, and guidelines for designing AirTouch-enabled objects. We illustrated AirTouch's flexibility with several applications, and showed that AirTouch is able to identify interactions with accuracies of at least 91% with 12 interactive locations.

ACKNOWLEDGEMENTS

We wish to thank Prof. Larry Villasmil from the Rochester Institute of Technology for his valuable input, and Mengyu Zhong for her help designing and fabricating test objects.

REFERENCES

1. Rafael Ballagas, Sarthak Ghosh, and James A Landay. 2018. The Design Space of 3D Printable Interactivity. *Proceedings of the ACM on Interactive, Mobile, Wearable and Ubiquitous Technologies* 2, 2 (July 2018), 61–21.
2. Daniel Bernoulli. 1738. *Hydrodynamica: sive de viribus et motibus fluidorum commentarii*. Johannis Reinholdi Dulseckeri.
3. Glenn O Brown. 2002. The History of the Darcy-Weisbach Equation for Pipe Flow Resistance. In *Environmental and Water Resources History Sessions at ASCE Civil Engineering Conference and Exposition 2002*. American Society of Civil Engineers, Washington, D.C., United States.
4. Géry Casiez, Nicolas Roussel, and Daniel Vogel. 2012. 1€ filter: a simple speed-based low-pass filter for noisy input in interactive systems. In *Proceedings of the SIGCHI Conference on Human Factors in Computing Systems*. ACM Press, New York, New York, USA, 2527.
5. Kristian Gohlke, Eva Hornecker, and Wolfgang Sattler. 2016. Pneumatibles: Exploring Soft Robotic Actuators for the Design of User Interfaces with Pneumotactile Feedback. In *Proceedings of the TEI '16: Tenth International Conference on Tangible, Embedded, and Embodied Interaction*. ACM, New York, New York, USA, 308–315.
6. Timo Götzelmann and Christopher Althaus. 2016. TouchSurfaceModels: Capacitive Sensing Objects through 3D Printers. In *Proceedings of the 9th ACM International Conference on PErvasive Technologies Related to Assistive Environments*. ACM, New York, New York, USA, 22–8.
7. Chris Harrison and Scott E Hudson. 2009. Providing dynamically changeable physical buttons on a visual display. In *Proceedings of the 2009 CHI Conference on Human Factors in Computing Systems*. ACM, New York, New York, USA, 299–308.
8. Liang He, Gierad Laput, Eric Brockmeyer, and Jon E Froehlich. 2017. SqueezaPulse: Adding Interactive Input to Fabricated Objects Using Corrugated Tubes and Air Pulses. In *International Conference on Tangible, Embedded, and Embodied Interaction*. ACM, New York, New York, USA, 341–350.
9. Jonathan Hook, Peter Wright, Thomas Nappey, Steve Hodges, and Patrick Olivier. 2014. Making 3D printed objects interactive using wireless accelerometers. In *CHI '14 Extended Abstracts on Human Factors in Computing Systems*. ACM, 1435–1440.
10. Charles Hudin, Sabrina Panëels, and Steven Strachan. 2016. INTACT: Instant Interaction with 3D Printed Objects. In *Proceedings of the 2016 CHI Conference Extended Abstracts on Human Factors in Computing Systems*. ACM, New York, New York, USA, 2719–2725.
11. Yvonne Jansen, Pierre Dragicevic, Petra Isenberg, Jason Alexander, Abhijit Karnik, Johan Kildal, Sriram Subramanian, and Kasper Hornbæk. 2015. Opportunities and Challenges for Data Physicalization. In *CHI '15: Proceedings of the 33rd Annual ACM Conference on Human Factors in Computing Systems*. ACM, New York, New York, USA, 3227–3236.
12. Shohei Katakura and Keita Watanabe. 2018. ProtoHole: Prototyping Interactive 3D Printed Objects Using Holes and Acoustic Sensing. In *CHI '18: Proceedings of the 36th Annual ACM Conference on Human Factors in Computing Systems*. ACM, New York, New York, USA, LBW112–6.
13. Seoktae Kim, Hyunjung Kim, Boram Lee, Tek-Jin Nam, and Woohun Lee. 2008. Inflatable mouse: volume-adjustable mouse with air-pressure-sensitive input and haptic feedback. In *Proceeding of the twenty-sixth annual CHI conference extended abstracts*. ACM, New York, New York, USA, 211–224.
14. Gierad Laput, Eric Brockmeyer, Scott E Hudson, and Chris Harrison. 2015. Acoustruments: Passive, Acoustically-Driven, Interactive Controls for Handheld Devices. In *CHI '15: Proceedings of the 33rd Annual ACM Conference on Human Factors in Computing Systems*. ACM, New York, New York, USA, 2161–2170.
15. Dingzeyu Li, David I W Levin, Wojciech Matusik, and Changxi Zheng. 2016. Acoustic voxels: computational optimization of modular acoustic filters. *ACM Transactions on Graphics (TOG)* 35, 4 (July 2016), 88–12.
16. Roderick Murray-Smith, John Williamson, Stephen Hughes, and Torben Quaade. 2008. Stane: synthesized surfaces for tactile input. In *CHI '08: Proceedings of the SIGCHI Conference on Human Factors in Computing Systems*. New York, New York, USA, 1299.

17. Kosuke Nakajima, Yuichi Itoh, Yusuke Hayashi, Kazuaki Ikeda, Kazuyuki Fujita, and Takao Onoye. 2013. Emoballoon. In *Advances in Computer Entertainment*. Springer, Cham, Cham, 182–197.

18. Ryuma Niiyama, Xu Sun, Cynthia Sung, Byoungkwon An, Daniela Rus, and Sangbae Kim. 2015a. Pouch Motors. *Soft Robotics* 2, 2 (June 2015), 59–70.

19. Ryuma Niiyama, Xu Sun, Lining Yao, Hiroshi Ishii, Daniela Rus, and Sangbae Kim. 2015b. Sticky Actuator. In *Proceedings of the 8th International Conference on Tangible, Embedded, and Embodied Interaction*. ACM Press, New York, New York, USA, 77–84.

20. Makoto Ono, Buntarou Shizuki, and Jiro Tanaka. 2013. Touch & activate: adding interactivity to existing objects using active acoustic sensing. In *UIST '13 Proceedings of the 26th annual ACM symposium on User interface software and technology*. ACM, New York, New York, USA, 31–40.

21. Jifei Ou, Mélina Skouras, Nikolaos Vlavianos, Felix Heibeck, Chin-Yi Cheng, Jannik Peters, and Hiroshi Ishii. 2016. aeroMorph - Heat-sealing Inflatable Shape-change Materials for Interaction Design. In *UIST '16: Proceedings of the 29th annual ACM symposium on User interface software and technology*. ACM, New York, New York, USA, 121–132.

22. Raf Ramakers, Fraser Anderson, Tovi Grossman, and George Fitzmaurice. 2016. RetroFab: A Design Tool for Retrofitting Physical Interfaces using Actuators, Sensors and 3D Printing. In *CHI '16: Proceedings of the 2016 CHI Conference on Human Factors in Computing Systems*. ACM, New York, New York, USA, 409–419.

23. Michel Rieutord. 2015. *Fluid Dynamics*. Springer International Publishing, Cham.

24. Jan Rod, David Collins, Daniel Wessolek, Thavishi Ilandara, Ye Ai, Hyowon Lee, and Suranga Nanayakkara. 2017. UTAP - Unique Topographies for Acoustic Propagation: Designing Algorithmic Waveguides for Sensing in Interactive Malleable Interfaces. In *International Conference on Tangible, Embedded, and Embodied Interaction*. ACM, New York, New York, USA, 141–152.

25. Harpreet Sareen, Udayan Umapathi, Patrick Shin, Yasuaki Kakehi, Jifei Ou, Hiroshi Ishii, and Pattie Maes. 2017. *Printflatables: Printing Human-Scale, Functional and Dynamic Inflatable Objects*. ACM, New York, New York, USA.

26. Valkyrie Savage, Colin Chang, and Björn Hartmann. 2013. *Sauron: embedded single-camera sensing of printed physical user interfaces*. ACM, New York, New York, USA.

27. Valkyrie Savage, Sean Follmer, Jingyi Li, and Björn Hartmann. 2015a. Makers' Marks: Physical Markup for Designing and Fabricating Functional Objects. In *UIST '15: Proceedings of the 28th annual ACM symposium on User interface software and technology*. ACM Press, New York, New York, USA, 103–108.

28. Valkyrie Savage, Andrew Head, Björn Hartmann, Dan B Goldman, Gautham Mysore, and Wilmot Li. 2015b. Lamello: Passive Acoustic Sensing for Tangible Input Components. In *CHI '15: Proceedings of the 33rd Annual ACM Conference on Human Factors in Computing Systems*. ACM Press, New York, New York, USA, 1277–1280.

29. Valkyrie Savage, Ryan Schmidt, Tovi Grossman, George Fitzmaurice, and Björn Hartmann. 2014. A series of tubes: adding interactivity to 3D prints using internal pipes. In *UIST '14: Proceedings of the 27th annual ACM symposium on User interface software and technology*. New York, New York, USA, 3–12.

30. Martin Schmitz, Mohammadreza Khalilbeigi, Matthias Balwierz, Roman Lissermann, Max Mühlhäuser, and Jürgen Steimle. 2015. Capricate: A Fabrication Pipeline to Design and 3D Print Capacitive Touch Sensors for Interactive Objects. In *UIST '15: Proceedings of the 28th annual ACM symposium on User interface software and technology*. ACM Press, New York, New York, USA, 253–258.

31. Martin Schmitz, Martin Stitz, Florian Müller, Markus Funk, and Max Mühlhäuser. 2019. ./trilaterate: A Fabrication Pipeline to Design and 3D Print Hover-, Touch-, and Force-Sensitive Objects. In *CHI '19: Proceedings of the 37th Annual SIGCHI Conference on Human Factors in Computing Systems*. ACM, New York, New York, USA, 454–13.

32. Lei Shi, Ross McLachlan, Yuhang Zhao, and Shiri Azenkot. 2016a. Magic Touch: Interacting with 3D Printed Graphics. In *Proceedings of the 18th International ACM SIGACCESS Conference on Computers and Accessibility*. ACM, New York, New York, USA, 329–330.

33. Lei Shi, Idan Zelzer, Catherine Feng, and Shiri Azenkot. 2016b. Tickers and Talker: An Accessible Labeling Toolkit for 3D Printed Models. In *CHI '16: Proceedings of the 2016 CHI Conference on Human Factors in Computing Systems*. ACM, New York, New York, USA, 4896–4907.

34. Ronit Slyper and Jessica Hodgins. 2012. Prototyping robot appearance, movement, and interactions using flexible 3D printing and air pressure sensors. In *2012 RO-MAN: The 21st IEEE International Symposium on Robot and Human Interactive Communication*. IEEE, 6–11.

35. Carlos Tejada, Osamu Fujimoto, Zhiyuan Li, and Daniel Ashbrook. 2018. Blowhole: Blowing-Activated Tags for Interactive 3D-Printed Models. In *Proceedings of the 44th Graphics Interface Conference GI Proceedings of the nd Graphics Interface Conference*. 122–128.

36. Marynel Vázquez, Eric Brockmeyer, Ruta Desai, Chris Harrison, and Scott E Hudson. 2015. 3D Printing

Pneumatic Device Controls with Variable Activation Force Capabilities. In *CHI '15: Proceedings of the 33rd Annual ACM Conference on Human Factors in Computing Systems*. ACM Press, New York, New York, USA, 1295–1304.

37. Karl Willis, Eric Brockmeyer, Scott E Hudson, and Ivan Poupyrev. 2012. Printed Optics: 3D Printing of Embedded Optical Elements for Interactive Devices. In *UIST '12: Proceedings of the 25th annual ACM symposium on User interface software and technology*. ACM Press, New York, New York, USA, 589–598.

38. Junichi Yamaoka, Ryuma Niiyama, and Yasuaki Kakehi. 2017. BlowFab: Rapid Prototyping for Rigid and Reusable Objects using Inflation of Laser-cut Surfaces. In *Proceedings of the 30th Annual ACM Symposium on User Interface Software and Technology*. ACM, New York, New York, USA, 461–469.

39. Lining Yao, Ryuma Niiyama, Jifei Ou, Sean Follmer, Clark Della Silva, and Hiroshi Ishii. 2013. PneUI: pneumatically actuated soft composite materials for shape changing interfaces. In *UIST '13 Proceedings of the 26th annual ACM symposium on User interface software and technology*. ACM, New York, New York, USA, 13–22.